Numerical Calculation of the Flow in a Centrifugal Pump Impeller Using Cartesian Grid

JOHN S. ANAGNOSTOPOULOS

School of Mechanical Engineering / Fluids Section
National Technical University of Athens
9 Heroon Polytechniou ave., Zografou, 15780 Athens
GREECE

Abstract: The simulation of the three-dimensional turbulent flow in turbomachines is currently based on the solution of the Reynolds Averaged Navier Stokes equations. A considerable computational effort usually goes to the mesh generation process due to the complexity of the impeller geometry. The use of Cartesian grids combined with a numerical technique for solving partially blocked cells is presented in this work. With the proposed approach the mesh generation can be accomplished very fast and in a fully automated way. The flow equations are discretized using the control volume approach, whereas the standard k-ε model is adopted for the turbulence closure. A number of geometric variables are introduced for the parameterization of the impeller geometry allowing also for easy design modifications. The computations for the steady flow field in a particular impeller are presented and the results are analyzed with the aid of 3-dimensional graphs. Next, the characteristic performance curves for the entire load range of the impeller are constructed, and their pattern is found reasonable and in agreement with theory.

Key-Words: Centrifugal pump impeller; Numerical modelling; RANS equations; Cartesian grids; Performance curves.

1 Introduction

Centrifugal pumps are prevalent for many different applications in the industrial or other sectors. Nevertheless, their design and performance prediction process is still a difficult task, mainly due to the great number of free geometric parameters, the effect of which cannot be directly evaluated. The significant cost and time of the trial-and-error process by constructing and testing physical prototypes reduces the profit margins of the pump manufacturers. For this reason CFD analysis is currently being used in hydrodynamic design for many different pump types [1-3].

The numerical simulation can provide quite accurate information on the fluid behaviour in the machine, and thus helps the engineer to obtain a thorough performance evaluation of a particular design. However, the challenge of improving the hydraulic efficiency requires the inverse design process, in which a significant number of alternative designs must be evaluated. Despite the great progress in the latest years, even CFD analysis remains rather expensive for the industry, and the need for faster mesh generators and solvers is imperative [4].

The mesh generation process is a laborious task for many CFD codes, and the quality of the final mesh depends considerably on the user's experience. An alternative practice in complex domains is the use of Cartesian grids that need a much reduced construction effort. However such grids cannot be everywhere body-fitted, and for this reason various numerical techniques have been developed to improve the accuracy in these regions [5-6].

A Cartesian mesh approach is also followed in the present work, where an advanced numerical technique is incorporated in order to eliminate the grid generation cost and to represent with adequate accuracy the complex geometry of a centrifugal pump impeller. The latter is parameterized using a reduced number of controlling geometric variables, facilitating the investigation of their individual or combined effects on the flow and the impeller performance. The results of the predicted flow field in the pump impeller illustrated in Fig. 1, as well as the numerically reproduced performance curves of the impeller are then presented and discussed.

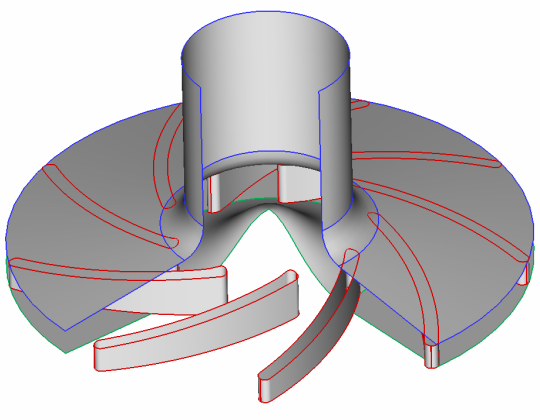

Figure 1. The examined radial impeller.

2 Numerical Method

2.1 Flow equations

The steady, incompressible, Reynolds Averaged Navier-Stokes (RANS) equations are employed for the flow calculations in polar coordinates and a rotating with the impeller system of reference. The governing conservation equations are expressed in vectorized form as follows:

Continuity: $$\nabla \cdot \vec{w} = 0 \qquad (1)$$

Momentum:

$$\vec{w} \cdot \nabla \vec{w} = -2\vec{\omega} \times \vec{w} + \omega^2 \cdot \vec{r} - \frac{1}{\rho} \cdot \nabla p + \frac{1}{\rho} \cdot \nabla \cdot \vec{\tau} \qquad (2)$$

where $\vec{w}$ is the relative fluid velocity, ω is the angular rotation speed of the impeller, $\vec{r}$ is the radial location and p, ρ are the fluid pressure and density, respectively. The viscous stress tensor $\vec{\tau}$ includes both the viscous and the turbulence viscosity terms:

$$\tau_{ij} = 2\mu \cdot s_{ij} - \overline{\rho \cdot w_i' \cdot w_j'} \qquad (3)$$

where μ is the fluid dynamic viscosity and s_{ij} is the strain tensor. The second term on the right side of the above relation represents the Reynolds stresses due to turbulent motion. Since the Reynolds number in a typical pump is high ($Re > 10^4$), the standard k-ε model is adopted for the turbulence closure [7], by solving additional conservation equations for the turbulence kinetic energy production, k, and its dissipation rate, ε.

All the dependent variables are stored at the cell centers of a uniform Cartesian mesh and the governing equations are discretized with the finite volume approach using a hybrid difference scheme. The system of the linearized form of the above equations is numerically solved by a preconditioned bi-conjugate gradient (Bi-CG) algorithm. Fully developed profile is assumed for the flow at the inlet tube and no-slip boundary conditions are applied at all internal solid surfaces. Due to the periodic symmetry of the impeller geometry, the computational domain can be restricted to a section of $2\pi/z$ degrees, where z is the number of blades, using periodicity boundary conditions at the lateral planes.

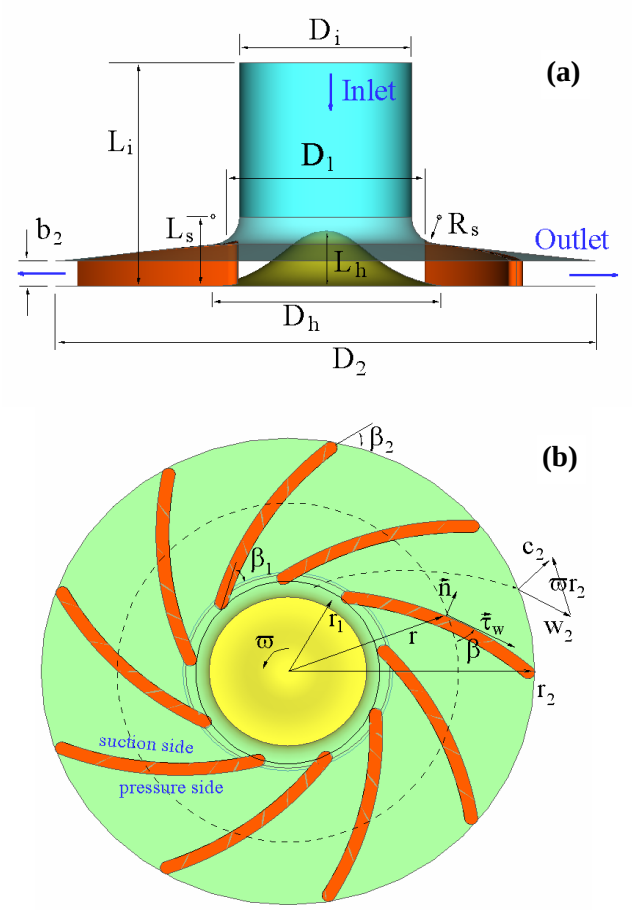

Figure 2. Parameterization of the impeller geometry: a) side view; b) top view.

2.2 Geometry parameterization

The geometry of the particular radial flow impeller examined here (Fig. 1) corresponds to a model impeller constructed in the Lab, and can be represented using a relatively small number of parameters; most of them are shown in Fig. 2 and their values are given in Table 1. The rotation speed and the main impeller dimensions, namely the exit diameter and width D_2 and b_2, as well as the blade inlet and exit angles, β_1 and β_2, respectively, determine the nominal head and volume flow rate of the impeller. The computational domain is extended to a certain radial distance beyond the impeller

outlet (here up to r = 125 mm, not shown in Fig. 2), to prevent any backward influence of the free vortex conditions set at the exit boundary.

The blades are constructed as circular arcs, and they have constant width and both edges rounded, allowing for both pump and turbine operation mode of the impeller. The rest parameters constitute the free design variables that can be modified in order to improve the performance and hydraulic efficiency of the impeller for this particular nominal operation point.

Table 1. Impeller dimensions.

Parameter	Size
Suction tube	D_i = 60 mm
Inlet diameter	D_1 = 70 mm
Exit diameter	D_2 = 190 mm
Exit width	b_2 = 9 mm
Hub size	D_h = 80 mm
Hub height	L_h = 20 mm
Shroud turn	R_s = 10 mm
Shroud turn	L_s = 25 mm
Blades number	9
Inlet angle	26 deg
Outlet angle	49 deg
Blade thickness	5 mm

2.3 Numerical grid

The important advantage from the use of Cartesian grids for complex geometries is the elimination of the computational effort and the automization of the grid generation process. However the grid lines can not in general fit in with the flow boundaries, therefore there are cells partly filled by the fluid that must be properly handled, as illustrated in the 2-dimensional example of Fig. 3.

The Partly-Filled-Cells (PFC) method is implemented for that purpose in the present work. It is a cell-cut, sharp-interface grid technique, developed and successfully tested in various applied studies in the past [8]. A desirable feature of the method is that the same general form of the linearized equations can be used for all the grid cells, regardless of their blocked portion.

The fluid variables (velocities, pressures, etc) are evaluated at the centroid of the Cartesian cells, which may not coincide with the geometric centre of a boundary cell (Fig. 3). All the necessary geometric quantities are automatically computed and the wall boundary conditions are set to every boundary cell (e.g. cells P_1 to P_4 in Fig. 3) with the aid of a special algorithm that computes the normal distance from the wall and the exact bounded area within each cell.

In addition to its simplicity and generality, that makes PFC method easily applicable to 3-dimensional geometries of any complexity, the conservation property is retained and the accuracy of the boundary representation remains satisfactory even with a coarse grid, and without affecting the stability of the solver.

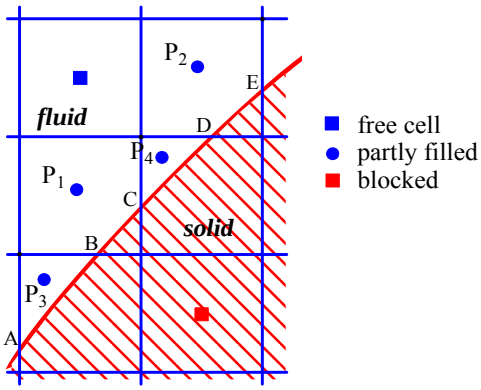

Figure 3. Example of the PFC grid method.

The numerical grid used for the present calculations has a number of approximately 200,000 nodes, which was found to be a good compromise between the results accuracy and the computation speed. An indicative picture of the grid configuration is given in Fig. 4 at the leading edge region of a blade.

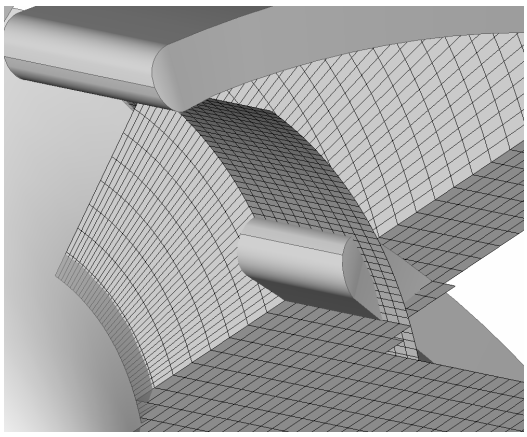

Figure 4. Detail of the grid lines arrangement

2.4 Hydraulic efficiency calculation

The hydraulic efficiency η_h of the impeller is defined as the ratio of the net energy added to the passing fluid, divided by the energy given at the impeller shaft. The specific energy (energy per unit fluid

weight) can be expressed by the corresponding heads, H and H_u, therefore the efficiency is given by:

$$\eta_h = \frac{H}{H_u} \tag{4}$$

The net fluid head H is obtained by energy balance at the inlet and the outlet of the impeller, using the following flux-weighted relation (Fig. 2b):

$$H = H_2 - H_1 = \frac{1}{Q_u} \cdot \int \left(\frac{p_2 - p_1}{\rho g} + \frac{c_2^2 - c_1^2}{2g} \right) \cdot dq \tag{5}$$

where c is the absolute velocity of the fluid, Q_u the volume flow rate through the impeller and g the gravity acceleration, while the subscripts 1 and 2 denote impeller inlet and exit conditions, respectively. The right-hand side integral is approximated by a summation over the radial flow rates δq at all grid cells facing the inlet or the exit circumference of the impeller.

The impeller head H_u can be calculated from the definition equation of the power absorbed at the shaft:

$$N_u = \rho \cdot g \cdot Q_u \cdot H_u \tag{6}$$

where N_u is analogous to the torque M_u developed on the impeller:

$$N_u = \omega \cdot M_u \tag{7}$$

The latter can be computed based on the conservation of angular momentum law, via the following relation (Fig. 2b):

$$M_u = \int_{r_1}^{r_2} \left[(\vec{r} \times \vec{n}) \cdot p + (\vec{r} \times \vec{\tau}_w) \cdot cot\, \beta \right] \cdot b \cdot dr + \int_A (\vec{r} \times \vec{\tau}_w) \cdot dA \tag{8}$$

where $\vec{n}$ is the local unit vector normal to the surface, $\vec{\tau}_w$ the wall shear stress, β the blade angle, and b the impeller width. The first integral term on the right represents the torque developed on the impeller blades due to the pressure and the friction forces, and includes both the pressure and the suction side of the blades. The second integral stands for the torque on the internal shroud and hub surfaces, and contains only the friction forces, since the pressure forces does not have a circumferential component.

3 Results

3.1 Flow analysis

At first the numerical model is applied to calculate the flow field developed in the standard impeller for various load conditions and a constant rotation speed of 1500 rpm. The 'nominal' volume flow rate is taken 31 m^3/h to comply with the corresponding laboratory model pump design conditions.

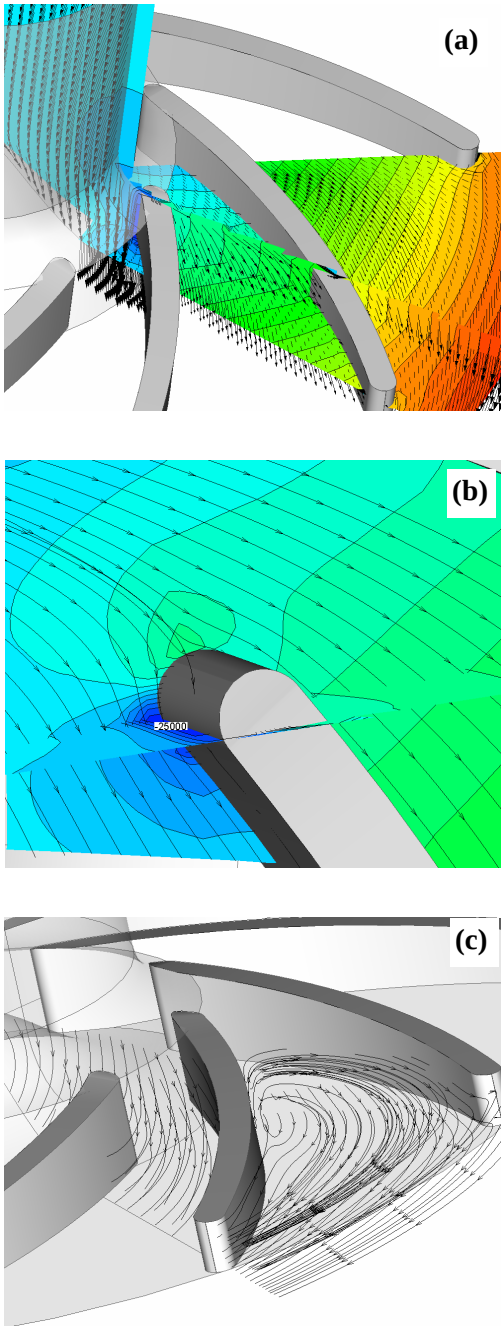

Figure 5. Flow field analysis for Q_u = 31 m^3/h: a) Pressure contours and velocity vectors; b) Stream lines and minimum pressure at the leading edge; c) Stream lines between the blades.

Fig. 5a shows the resulting contours of pressure and the velocity vectors at two grid levels that cross the impeller normal to- and through its axis of

rotation. Increased flow velocity can be observed at the blade inlet due to the blockage of the flow, whereas on the contrary the pressure is reduced. Further downstream the pressure contours become smooth between the blades and its value increases continuously towards the exit of the computational domain.

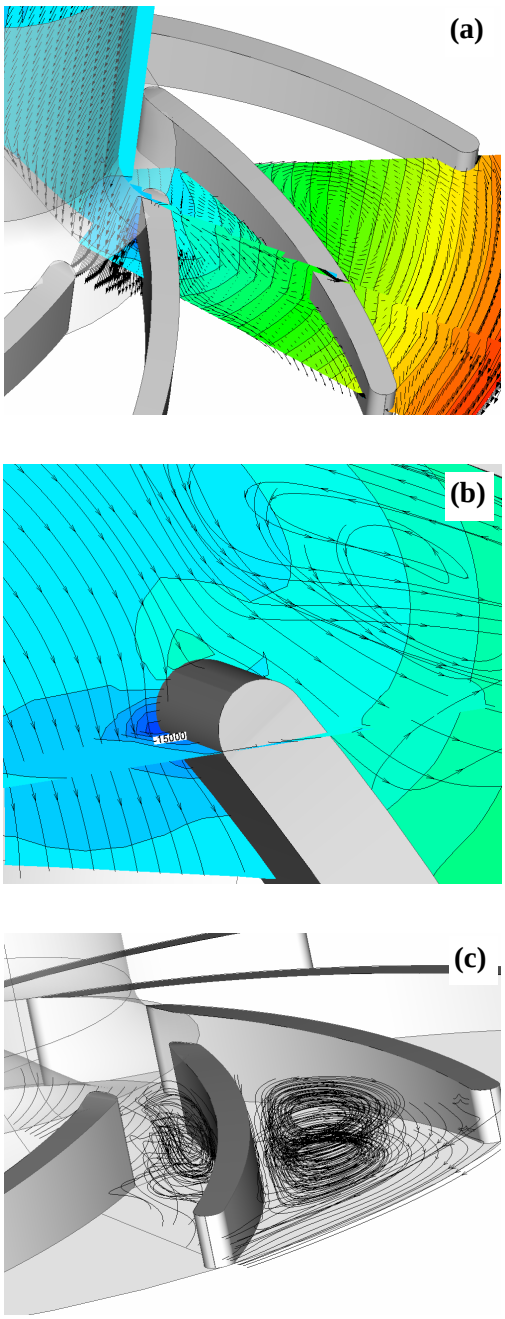

Figure 6. Flow field analysis for Q_u = 6,2 m^3/h. Legend as in Fig. 5.

The minimum pressure appears, as expected, at the suction side and near the leading edge of the blade (Fig. 5b). The flow seems to enter almost parallel to the blade (Fig. 5b) and the streamlines follow a regular pathway between the blades, except of the upper section near the shroud where some recirculation can be observed (Fig. 5c).

Fig. 6 illustrates the corresponding flow field for a much reduced flow rate, equal to 20% of the 'nominal'. The different flow characteristics can be clearly observed: the pressure gradients are lower throughout the domain and the minimum values are higher (Fig. 6a,b). However, a strong recirculation is established within almost the entire blade-to-blade region, which according to the theory rotates in the reverse direction from the impeller.

The results for the case of a double volume flow rate (62 m^3/h) were finally obtained and are shown in Fig. 7. Now the pressure and the velocity fields exhibit higher gradients but no important recirculation is observed in the impeller (Fig. 7a). However, due to the higher radial flow velocity at the blades inlet, the stagnation line is moved towards the suction side of the blade leading edge, and consequently the minimum pressure is displaced to the opposite pressure side (Fig. 7b).

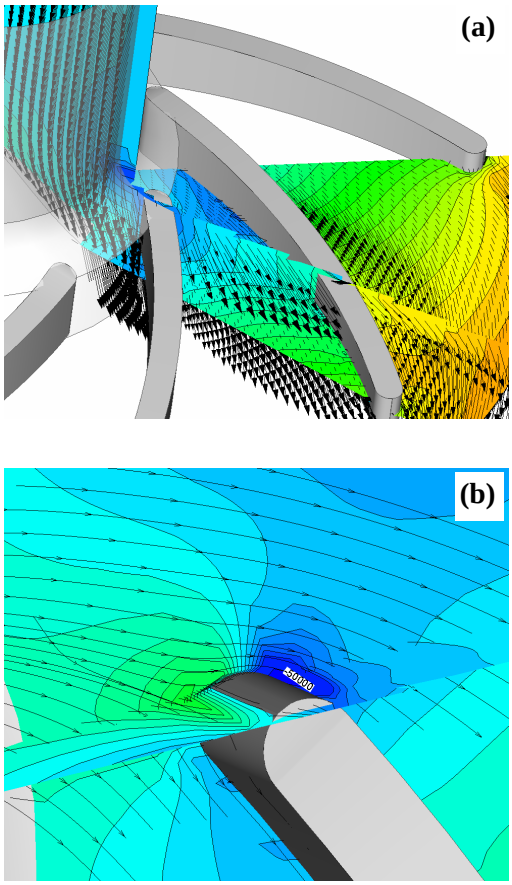

Figure 7. Flow field analysis for Q_u = 62 m^3/h.

3.2 Impeller performance

The numerical model is then applied to reproduce the performance characteristic curves of the standard impeller at 1500 rpm, covering the entire load range from 20% to 200% of the 'nominal' value. The computed curves are drawn in Figs. 8a and 8b and the first observation is that the maximum hydraulic efficiency is achieved for Q ≈ 22,5 m^3/h, which is lower than the 'nominal' value. However, a better estimation of the latter for the simulated geometry with the aid of the inlet triangle of velocity vectors gave the value of about 25 m^3/h.

The net fluid head and the impeller power curves, plotted in Figs. 8a and 8b, respectively, exhibit a reasonable and smooth pattern, verifying the reliability of the PFC grid technique. As expected, an increase of the volume flow rate above a safety limit deteriorates the suction characteristics of the impeller. The minimum pressure values in Fig. 8b are drastically reduced for Q > 50 m^3/h, indicating that intense cavitation may occur in the impeller.

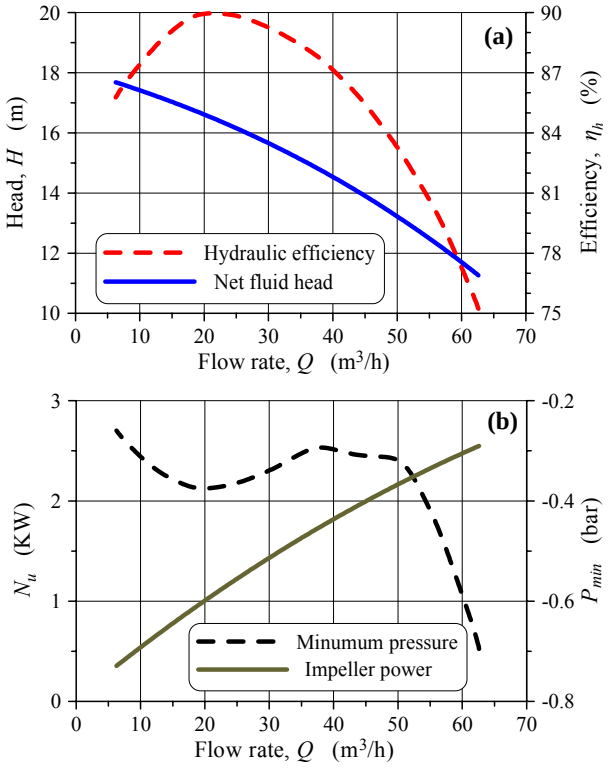

Figure 8. Impeller performance curves.

4 Conclusions

A numerical model is developed for the numerical solution of the RANS equations in the impeller of a centrifugal pump, and it is applied for a direct flow analysis and for the prediction of the impeller characteristic operation curves.

The use of properly defined geometric parameters to describe the impeller shape, along with the automatic grid generation process of the present model, constitute a useful tool for the investigation of the effects of the impeller geometry on its hydrodynamic performance and hydraulic efficiency.

Acknowledgement:
The project is co-funded by the European Social Fund (75%) and National Resources (25%) – Operational Program for Educational and Vocational Training II and particularly the Program Pythagoras.

References:

[1] C. Hornsby, CFD – Driving pump design forward, *World Pumps*, August 2002, pp. 18-22.

[2] S. Cao, G. Peng, and Z. Yu, Hydrodynamic design of rotodynamic pump impeller for multiphase pumping by combined approach of inverse design and CFD analysis, *ASME Transactions, Journal of Fluids Engineering*, Vol.127, 2005, pp. 330-338.

[3] F.A. Muggli and P. Holbein, CFD calculation of a mixed flow pump characteristic from shutoff to maximum flow, *ASME Transactions, Journal of Fluids Engineering*, Vol.124, 2002, pp. 798-802.

[4] M. Asuaje, F. Bakir, S. Kouidri, and R. Rey, Inverse design method for centrifugal impellers and comparison with numerical simulation tools, *International Journal for Computational Fluid Dynamics*, Vol.18, no.2, 2004, pp. 101-110.

[5] T. Ye, R. Mittal, H.S. Udaykumar, and W. Shyy, An accurate Cartesian grid method for viscous incompressible flows with complex immersed boundaries, *Journal of Computational Physics*, Vol.156, 1999, pp. 209-240.

[6] E.A. Fadlun, R. Verzicco, P. Orlandi, and J. Mohd-Yusof, Combined immersed-boundary finite-difference methods for three-dimensional complex flow simulations, *Journal of Computational Physics*, Vol.161, 2000, pp. 35-60.

[7] T.J. Chung, *Computational Fluid Dynamics*, Cambridge University Press, UK, 2002.

[8] J. Anagnostopoulos and D. Mathioulakis, A flow study around a time-dependent 3-D asymmetric constriction, *Journal of Fluids and Structures*, Vol.19, 2004, pp. 49-62.